NJC

Accepted Manuscript

This is an *Accepted Manuscript*, which has been through the RSC Publishing peer review process and has been accepted for publication.

Accepted Manuscripts are published online shortly after acceptance, which is prior to technical editing, formatting and proof reading. This free service from RSC Publishing allows authors to make their results available to the community, in citable form, before publication of the edited article. This *Accepted Manuscript* will be replaced by the edited and formatted *Advance Article* as soon as this is available.

To cite this manuscript please use its permanent Digital Object Identifier (DOI®), which is identical for all formats of publication.

More information about *Accepted Manuscripts* can be found in the **Information for Authors**.

Please note that technical editing may introduce minor changes to the text and/or graphics contained in the manuscript submitted by the author(s) which may alter content, and that the standard **Terms & Conditions** and the **ethical guidelines** that apply to the journal are still applicable. In no event shall the RSC be held responsible for any errors or omissions in these *Accepted Manuscript* manuscripts or any consequences arising from the use of any information contained in them.

Journal Name

RSCPublishing

ARTICLE

Effect of the Different Synthetic Parameters on the Morphology and Magnetic Properties of Nickel Nanoparticles

Cite this: DOI: 10.1039/x0xx00000x

Received 00th January 2012,
Accepted 00th January 2012

DOI: 10.1039/x0xx00000x

www.rsc.org/

Veronica Paredes-Garcia,[*a,b] Carlos Cruz,[b] Nestor Toledo,[b] Juliano Denardin,[b,c] Diego Venegas-Yazigi,[b,d] Carolina Castillo,[b,e] Evgenia Spodine[b,e] and Zhiping Luo[f,g]

Coated stable metallic nickel nanocrystals (fcc-Ni) forming micro and nano aggregates with different morphologies have been synthesized through a one-pot N^{iII} reduction process in presence of L-serine (Ni-1 to Ni-5). The subsequent warming under solvothermal conditions of the spherical nickel particles (Ni-1) with ethylenglycol (EG) modifies the morphology of the initial spheres to hexagonal-quasi circular plates, which are disposed as a 3D arrangement (Ni-4). Electron microscopy images indicate that the size of these aggregates is 2 μm, being the thickness of the plates, c.a. 110-200 nm. The magnetic measurement results for Ni-4 show a ferromagnetic behaviour with both an enhanced coercivity (92 Oe) and magnetic remanence (7 emu g^{-1}), and lower magnetic saturation (43 emu g^{-1}), as compared with bulk nickel. The enhancement of the ferromagnetic properties observed for all the studied NPs is attributed to the dependence on the shape anisotropy and dipolar interactions.

Introduction

During the past decades, the synthesis of micro- or nano-sized metallic particles has been an important research field because of their unique physical and chemical properties, which differ considerably from those of bulk materials.[1] Different metallic systems in the scale of micrometric or nanometric dimensions have been synthesized and studied, obtaining fascinating and interesting mechanical, electrical and magnetic properties.[2]

From a magnetic point of view, the particles with sizes in the nanometer scale are now of great interest, because of their many technological applications. Special attention has been given to the nanoscale metal-based materials, such as Ni, Co and Fe.[3] Many studies about the magnetic properties of small aggregates, nanowire arrays and single molecule magnets have been published.[4] Through these studies it was possible to find that below a critical size, the magnetic particles become single domain, in contrast with the usual multidomain structure of the bulk magnetic materials, exhibiting phenomena such as superparamagnetism and quantum tunneling of the magnetization.[4]

Magnetic nanoparticle systems with superparamagnetic behavior, display little or no remanence and coercivity while keeping a high value of the saturation magnetization. Depending of the type of transition metal ion, they have potential application in biomedicine,[5] drug delivery and cell-sorting systems[6] or in magnetic refrigeration technology.[7]

On the other hand, a number of physical and chemical routes, such as the thermal decomposition of an organometallic precursor, the chemical reduction method and the arc-charge spilling route, have been applied to prepare transition metal nanocrystals.[8] Nowadays, due to recent advances in experimental techniques one can synthesize, characterize and design special materials with specific size, composition and structure. It is interesting that these new materials show unexpected physicochemical properties that are not interpolations of those shown by the atomic or molecular structures and the bulk solids. These effects are recognized to be produced mainly by the large amount of superficial atoms.[9]

Some transition metal micro or nanocrystals are difficult to be prepared due to their highly oxidizing capacity. Therefore, different matrices have been used as protective surfaces against air-oxidation; such is the case of metallic nickel which has been encapsulated in inert matrices as graphite,[10] fullerene[11] or in oxide-type matrices like zeolites,[12] alumina,[13-14] titanium dioxide[15] or silica ones.[16] Furthermore, the hydrothermal approach has been also used for the preparation of micro- and nanosized metallic systems, such as Co, Ni and Ru.[3,17]

In this work a one pot solvothermal method, which permits an in-situ reduction to Ni^0 nanoparticles, with spherical o cubic-like

morphology is being reported. This method permits to obtain directly from a Ni^{II} salt and L-serine, pure organic coated nickel particles, which are air stable. Furthermore, the subsequent heating of the nickel spheres modifies the spherical morphology, organizing 3D platelet aggregates with flower like form. Magnetic characterization of the spherical, cubic and 3D platelet aggregates of Ni^0 particles is also reported.

Experimental

Synthesis

All starting materials were commercially available reagents of analytical grade (Merck), and were used without further purification. The solids **Ni-1** and **Ni-2** were obtained by solvo/hydrothermal synthesis from L-2-amino-3-hydroxipropanoic acid (L-serine) and $NiCl_2{\cdot}4H_2O$ in a molar ratio of 1:1, using DMF (**Ni-1**) or water (**Ni-2**) in a 23 mL Teflon-lined stainless steel autoclave. The reactor was heated at 150 ^oC for 24 h under self-generated pressure. After slow cooling (0.05 ^oC/min) to room temperature, the solid product was filtered and dried at 40 ^oC. A similar synthetic procedure was used to obtain **Ni-3**, but in this case a molar ratio of 1:2 of the reagents together to the use of $Ni(OAc)_2{\cdot}4H_2O$ as metal source, was considered. **Ni-4** was obtained by direct heating of solid **Ni-1** in a Teflon-lined stainless steel autoclave, using a ratio of 4:1 DMF:EG (Merck), at 150 ^oC for 24 hours, while **Ni-5** was prepared using the same experimental conditions as for **Ni-1** and the same solvent mixture used to generate **Ni-4**. Table 1 summarize the synthetic details of each obtained product.

Table 1: Synthetic data of the products

Sample	Method	Solvent	Metal source
Ni-1	Solvothermal	DMF	$NiCl_2{\cdot}4H_2O$
Ni-2	Hidrothermal	H_2O	$NiCl_2{\cdot}4H_2O$
Ni-3	Solvothermal	DMF	$Ni(OAc)_2{\cdot}4H_2O$
Ni-4	Re-Heating	DMF:EG	Ni-1
Ni-5	Solvothermal	DMF:EG	$NiCl_2{\cdot}4H_2O$

Equipment and characterization techniques

X-Ray Powder Diffraction. Compounds Ni-1 to Ni-5 were analyzed by powder X-ray diffraction using a Siemens D5000 equipment, with Cu-Kα_1 radiation and Bragg-Brentano geometry in the $5^o \leq 2\theta \leq 80^o$ range. The analyses were performed using directly the microcrystalline samples. Electron Microscopy and X-ray Spectroscopy. The morphology, composition, crystal structure and size distribution of the samples were identified by using a Zeiss EVO MA 10 scanning electron microscope (SEM), a JEOL-JEM 6400 (SEM) with coupled energy dispersive X-ray spectroscopy (EDXS), and transmission energy microscopy (TEM) JEOL 2010 with Oxford EDS detector with atmospheric thin windows, which is capable of detecting elements with $Z \geq 5$. In order to make accurate size measurements, the magnifications were calibrated using SiC lattice fringes.[18] FTIR and DRIFT Spectroscopy. Absorption infrared and diffuse reflectance infrared spectra were recorded at room temperature on a Perkin Elmer Spectrum BXII spectrophotometer. The infrared spectra were recorded in the 4000–400 cm^{-1} range using KBr pellets. DRIFT spectra were obtained on solid samples in the 4000-400 cm^{-1} range, on solid samples, in order to determine the presence of organic coating on the metallic solids. Magnetic Characterization. The magnetization curves of the synthesized metallic nickel nanoparticles were recorded at room temperature on a vibrating sample magnetometer (VSM).

Results and discussion

Synthesis

Ni^0 particles were obtained by a reductive method from Ni^{II} salts and the amino acid L-serine, using a solvo/hydrothermal process, under mild temperature conditions. The synthesis of solid **Ni-1** and **Ni-2** was carried-out under similar experimental conditions. In both cases, the reagents were used in the same stoichiometry and solvent volume, but DMF was used for the preparation of **Ni-1** and water for **Ni-2**. Although in both solvents it is possible to obtain Ni^0, the yield of the metallic product with DMF as solvent is greater (76 %), than the one obtained in water as solvent (13 %). Furthermore, in product **Ni-2** a significant amount of impurities was observed, making difficult the separation of the metallic phase from the bulk. The changes in the stoichiometry of the reagents used for the preparation of **Ni-3** have no influence on the type and yield of the final product. **Ni-4** was obtained by heating **Ni-1** in a Teflon-lined stainless steel autoclave using a mixture of DMF and ethylene glycol as solvent. **Ni-5** was obtained considering this same solvent mixture, L-serine and $NiCl_2{\cdot}4H_2O$ as starting materials. These syntheses were done with the purpose to produce modifications in the size and/or the morphology of the metallic particles.

Energy dispersive X-ray and diffuse reflectance FTIR spectroscopy

EDXS analyses performed on microcrystalline samples of **Ni-1** to **Ni-5** showed mainly the presence of nickel in the samples (Figure 1S and 2S). An EDXS detector for chemical analysis of elements with $Z \geq 5$ was used to determine the chemical composition of **Ni-1**. The EDX result shows that **Ni-1** (Figure 1S) is composed mainly by nickel; a lower percentage of carbon is also identified. Although oxygen was detected in the sample, the percentage is too low to consider that the oxidation of Ni^0 to nickel oxide could be occurring. Moreover, the oxygen can also be associated to the presence of the amino acid coating, or some derivative of this, in the sample. The presence of small amounts of the other elements which are not considered in the initial conditions of the synthesis can be attributed to contamination in the preparation of the sample. Infrared and diffuse reflectance infrared spectroscopy were used to analyse the synthesized

metallic phases. IR absorptions due to organic components were not observed in the FTIR spectra obtained for **Ni-1** to **Ni-5**. Besides absorptions at values lower than 500 cm^{-1}, attributed to Ni-O bond vibration were not observed; being **Ni-2** the only sample to show bands in this zone. DRIFT analyses of **Ni-1**, **Ni-2, Ni-3, Ni-4** and **Ni-5** (Figure 3S) show in all cases very weak and wide absorptions at 1625 and 1500 cm^{-1}, which can be associated to the presence of carboxylate groups of the amino acid present as coating.[19] Furthermore, considering the presence of some organic compounds in the synthesized metallic phase, all samples were analyzed by elemental analysis for carbon, obtaining values between 5.0 and 7.0 % for the samples.

X-Ray powder diffraction

In order to determine the chemical composition and crystallinity of the synthesized metallic phases, X-ray powder diffraction was used. Figure 1 shows the X-ray powder diffraction plot obtained for **Ni-1** to **Ni-5**. Only three peaks at 2θ of 44.48, 51.84 and 76.44 ° are observed for **Ni-1**, **Ni-3**, **Ni-4** and **Ni-5**. The observed position and the intensity of these diffraction peaks can be correlated with the crystal planes (111), (200) and (220) at 2θ of 44.496, 51.849, and 76.381° respectively, corresponding to face centred cubic *fcc*-Ni^0 (JCPDS Card 04-0850, cubic system, spatial group: $Fm\bar{3}m$, a=3.5238 Å). No additional peaks associated to impurities or the presence of the hexagonal close packed phase (*hcp*) of Ni^0 were observed. The powder diffraction pattern obtained for **Ni-2** also shows the same three peaks which permit to infer that *fcc* Ni^0 is also present in this sample. However, other peaks at 2θ values lower than 30° were observed, indicating the presence of impurities in the sample; these peaks being attributed to the presence of oxidized species. It is important to note that **Ni-1**, **Ni-4** and **Ni-5** have the same powder diffraction pattern, indicating that no changes in the chemical identity occur, by heating under solvothermal conditions or by the adding of EG to the reaction mixture. It is important to note that subsequent measurements done during one month show no variations in the diffraction patterns of **Ni-1**, **Ni**-3, **Ni-4** and **Ni-5**. Therefore, taking into account the results obtained from X-ray powder diffraction, together with the obtained from EDX, elemental analysis and DRIFT, it is possible to infer that the synthesized metallic solids have an organic coating which permits to explain the greater stability of the Ni^0 particles to air oxidation.

Based on the fact that **Ni-2** shows impurities and a very low yield, we only considered for the subsequent analysis the **Ni-1**, **Ni-3, Ni-4** and **Ni-5** samples. The mean size of the Ni^0 particles was obtained in a first approach by using the Scherer formula (eq. 1)[20]:

$$D = \frac{0.9\lambda}{\beta \cos\theta} \qquad (1)$$

where D corresponds to the mean size, λ is the X-ray wavelength, β is the line broadening at half the maximum intensity, and θ is the Bragg angle.

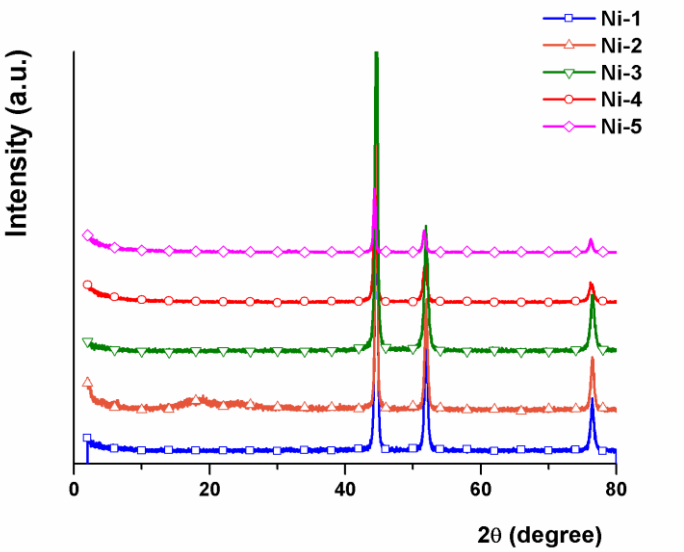

Figure 1: Powder diffraction pattern of Ni^0 particles. □ = Ni-1; △= Ni-2; ▽= Ni-3; ○= Ni-4; ◇ = Ni-5.

Based on the maximum intensity peak for the (111) crystal plane of the three samples, the mean size obtained from the Scherer equation was 20 nm for **Ni-1**, 22 nm for **Ni-3**, 15 nm for **Ni-4** and 25 nm for **Ni-5**.

TEM and SEM microscopy

The morphology and size of the particles was analysed by the SEM and TEM techniques. The SEM and TEM images of **Ni-1, Ni-3, Ni-4** and **Ni-5** at different magnifications are shown in Figures 2-6. The SEM images of **Ni-1** (Figure 2) show Ni^0 particles with quasi-spherical shapes which appear to aggregate together along one direction, forming flowering wood-like features in **Ni-1**.

A higher resolution for these metallic particles was obtained by TEM microscopy (Figure 3a-3f). The images show different aggregates which are formed by smaller particles. Two representative areas labelled as 1 and 2 were analysed in the sample, with consecutively increased magnifications. As shown in Fig. 3b, basically two features are identified; one is the larger particles which serve as sketch of the flower and the other corresponds to smaller particles which serve as the petals. Figure 3c, is a magnified image of area 1, with an inset of an electron diffraction pattern (EDP) from this area, showing a single-crystal Ni^0 *fcc* structure along [011], which is consistent with the XRD results. A magnified image from the framed area in 3c is given in 3d.

On the other hand, in area 2 as shown in Fig. 3e the EDP exhibits poly-rings indicative of the presence of nickel nanocrystals in the sample. An enlarged image from the red frame shows Ni^0 nanoparticles (Figure 3f). Measurements of the nanoparticle size give an average of 18.4 nm with standard deviation of 5.0 nm, which is consistent with the XRD results. EDXS analysis for the indicated yellow circled area from the sketch part shows primarily the presence of Ni, but also a low concentration of C

and O is determined (Figure 2Sa). The EDXS for the yellow circled area from the petal area (figure 3f), also shows primarily Ni and also a coating with C and O elements (Figure 2Sb).

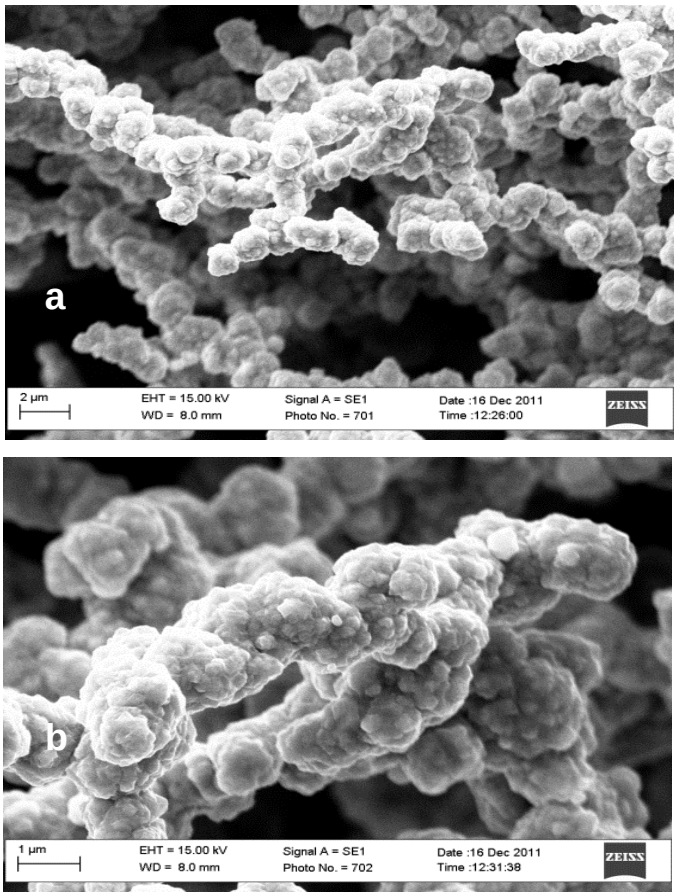

Figure 2: SEM images of **Ni-1** at two different magnifications.

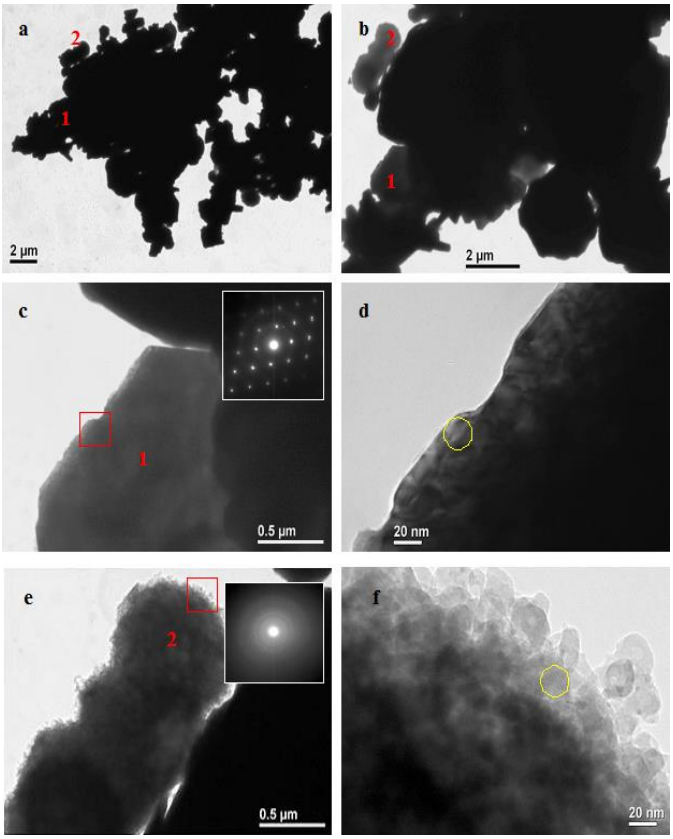

Figure 3: TEM images of **Ni-1.** (a) and (b): two representative areas at different magnifications labelled as (1) and (2); (c) greater magnification of area 1 with its diffraction pattern; (d) magnified image from the framed area in (c); (e) greater magnification of area (2) with its diffraction pattern and (f) magnified image from the framed area 2 in (e).

SEM images obtained at two magnifications, for **Ni-3** are given in Figure 4 showing small aggregates with quasi-cubic shapes. If the **Ni-3** SEM images are compared with SEM images obtained for **Ni-1**, different size and morphology are evidenced for the synthesized Ni^0 particles. In the case of **Ni-3**, smaller particles with homogeneous distribution can be observed, indicating the relevance of the experimental conditions; the nature of the anion of the metallic salt and the molar ratio permit to modify the visual characteristics of the particles.

The change in the morphology of the **Ni-1** particles, obtained by heating them in DMF/EG can be evidenced by the SEM images obtained for **Ni-4** (Figure 5). In these images it is possible to observe that the quasi-spherical forms of the synthesized Ni^0 particles obtained in **Ni-1** are completely changed to hexagonal quasi-circular plates. The plates are arranged in such a way that a shape similar to the petals of a flower is adopted (Figure 5). Due to the spatial arrangement of the plates it was difficult to estimate their size; the length value is in the range of 2 µm and the thickness varies between 110 to 200 nm, approximately. Nevertheless, if the mixture DMF/EG is used as solvent in the reduction process of Ni^{II} only spherical Ni^0 particles were observed (Figure 6), which are different from those obtained for **Ni-1**. Clearly Ni^0 chains observed in **Ni-1** (Figure 2) are not observed in **Ni-5** (figure 6) where only isolated polyhedrons of Ni^0 nanoparticles with a size of ~200 nm are evidenced. The SEM images also show in some cases particles with well-defined faces (Figure 6b). This result permits to infer that the use of EG permits to change the morphology of the particles and also avoids the trend to coalesce of the magnetic nanoparticles.

Similar 3D arrangement morphologies for Ni^0 particles, obtained by different synthetic methods has been reported in the literature, and the size of the flower-like particles varies between 200 nm to 2 µm approximately;[21-27] this last size being similar to the one obtained in this work. Some formation mechanisms of the Ni^0 flower-like architectures have been proposed, considering in a first stage the formation of spheres, determined by the lowest energy principle,[28] which are later transformed into plates.[22,27] The proposed mechanism by Guan et al.[22] for the nickel flower-like particles is based on the fact that a preferential growth direction of a magnetic crystalline phase is determined by the minimization of the sum of the magnetic anisotropic energy and the surface free energy.

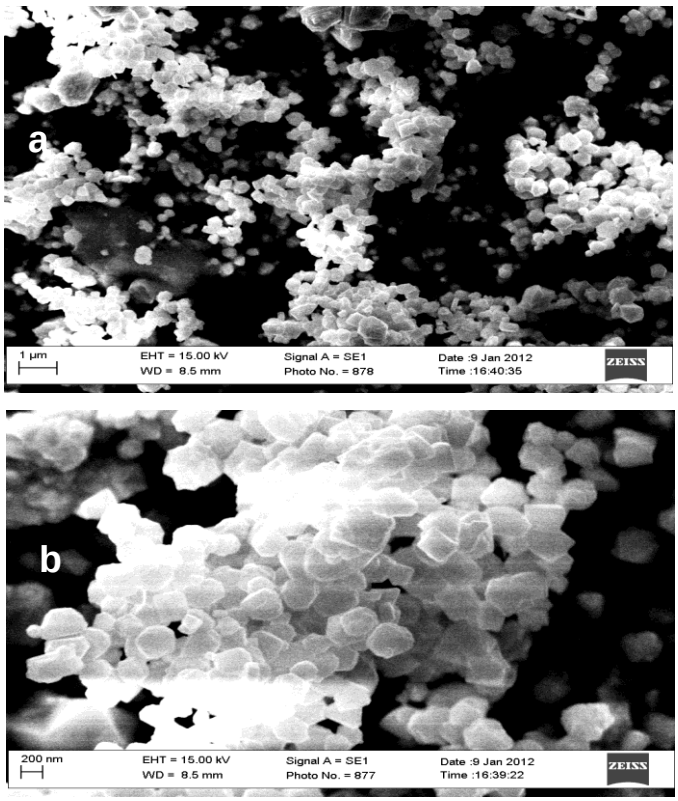

Figure 4: SEM images of **Ni-3** at two different magnifications.

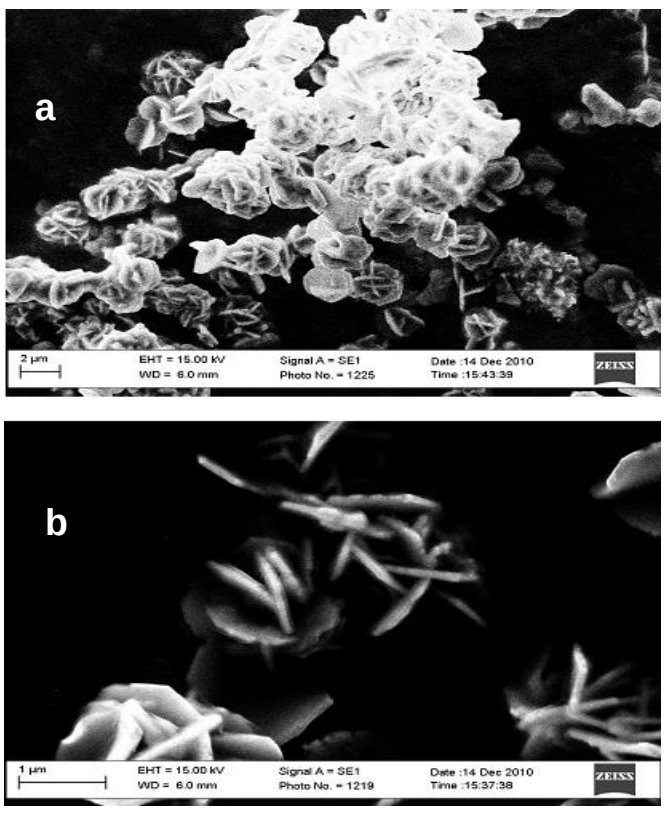

Figure 5: SEM images of **Ni-4** at two different magnifications.

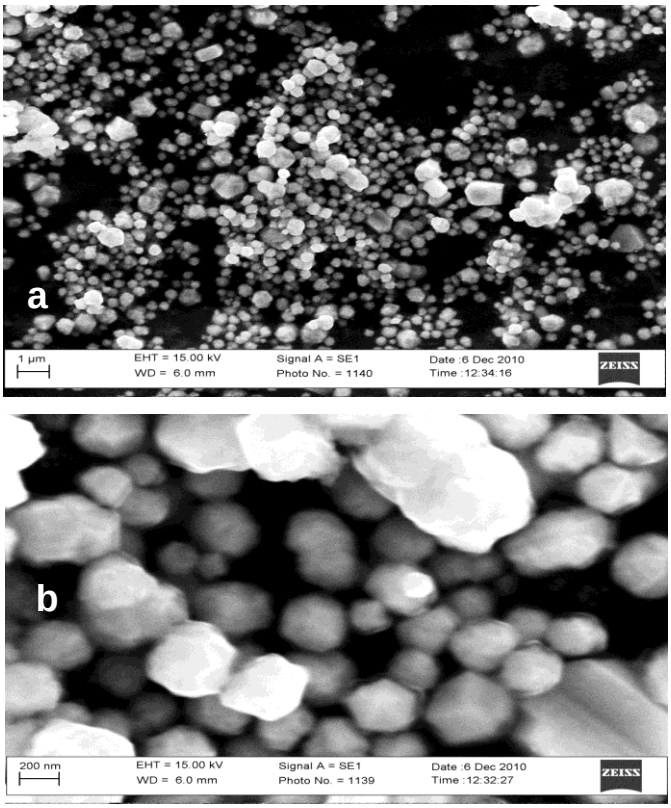

Figure 6: SEM images of **Ni-5** at two different magnifications.

The former shows a minimum value when the growth is along the magnetic easy axis, while the latter has a lower value if the growth is along the normal direction of high energy crystalline facets.[22] In the case of magnetic nickel with fcc structure, the magnetic easy axis is (111), and is different from the normal directions of the high energy crystalline facets; therefore the crystal growth occurs preferentially along the (110) and/or (100) directions, generating the top/bottom faces of the (111) planes with the lowest surface energy.[22,27,29]

Although, this mechanism is proposed for the flower-like morphology for Ni^0 obtained directly as a product of synthesis, it can also be used to explain the flower-like morphology observed when the synthesized spherical Ni^0 particles (**Ni-1**) are heated under solvothermal conditions, using EG/DMF as solvent. However, the role of the solvent should also be considered in the mechanism, because when **Ni-1** is heated without using DMF, no changes in the morphology were observed. Moreover, to the best of our knowledge, for the first time Ni^0 nanoflowers have been obtained from previously synthesized spherical Ni^0 particles.

It is important to note that using different experimental conditions it is possible to obtain Ni^0 particles with different shapes and with sizes lower than 200 nm. The high magnification electron microscopy images indicate that the larger Ni^0 particles are formed by smaller Ni^0 nanoparticles, a fact which is also in agreement with the XRD results.

Magnetic measurements

The magnetization curves of the synthesized Ni^0 nanoparticles were measured at room temperature using 6.0 kOe as the maximum applied field. Hysteresis loops $M(H)$ of **Ni-1, Ni-3, Ni-4** and **Ni-5** are shown in Figure 7. The magnetization hysteresis loops show in all cases a ferromagnetic behaviour for the synthesized Ni^0 particles, obtaining H_c values of 120 for **Ni-1**, 200 for **Ni-3**, 98 for **Ni-4** and 73 Oe for **Ni-5**. The remanent magnetization (M_r) is 5 for **Ni-1**, 10 for **Ni-3**, 7 for **Ni-4** and 4 emu g^{-1} for **Ni-5**. Clearly, the H_c and M_r values obtained for the synthesized Ni^0 nanoparticles are significantly higher, than those reported for bulk nickel (H_c ~ 0.7 Oe, M_r ~2.7 emu g^{-1}).[21] On the other hand, the magnetic saturation for the three samples is achieved at external magnetic field values greater than 4 kOe, giving values of 50, 51, 42 and 45 emu g^{-1} for **Ni-1**, **Ni-3**, **Ni-4** and **Ni-5** respectively; these values being lower than that observed for bulk nickel (M_s ~ 55 emu g^{-1}).[21] It is important to note that no change in the magnetic parameters were evident for **Ni-1**, **Ni**-3, **Ni-4** and **Ni-5,** when the samples were re-measured one month later. Thus the magnetic parameters, together with the diffraction data, permit to infer that no important chemical transformation occurred during this period.

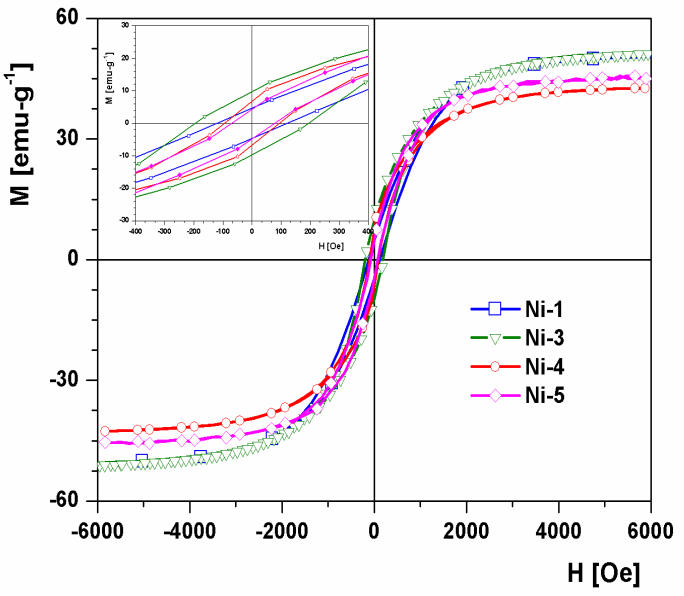

Figure 7: Hysteresis loops for the synthesized nickel nanoparticles. □ = Ni-1; ▽= Ni-3; ○= Ni-4; ◇ = Ni-5.

As it is well known, the magnetic properties of nanomaterials are related to the composition, crystallinity, size and morphology. The SEM images show that the samples have different shapes, which affect the anisotropy and the dipolar interactions, and significantly modifying the magnetic properties.[29,30] Thus, comparing the magnetic parameters of the bulk metal with the as prepared Ni^0 nanoparticles, the enhanced coercivity magnetization observed for the nanoparticles can be attributed to the decrease of the size, and/or to the different shapes of the nanocrystals, which are forming the different aggregates.[25,31-33]

As the size and the shape of the nanoparticles are different, these nanoparticles should also present different surface specific areas. Thus, if we compare the H_c and M_r of the as synthesized nickel NPs, **Ni-1** and **Ni-3**, and taking into account that the sizes of the particles obtained from DRX measurements are very similar, 20 and 22 nm respectively, we can attribute the higher values of the coercivity and remanent magnetization of **Ni-3,** to the different shape of the aggregates, i.e spherical-like in the case of **Ni-1** and cubic-like for **Ni-3**. Besides, comparing the values obtained for **Ni-1** and **Ni-5**, where in both cases the isolated Ni^0 particles with similar sizes but different shapes were obtained (**Ni-**1=20 nm; **Ni-5**= 25 nm), the lower values of the H_c and M_r are obtained for **Ni-5,** where polyhedrons with well-defined faces are observed. Moreover, the difference between the coercivity of **Ni-1** and **Ni-4** cannot only be attributed to the smaller size of Ni^0 nanoparticles forming **Ni-4** (15 nm) but also to their shape. Literature reports that the nanoplates, which are forming the flower-like aggregates of **Ni-4**, should present a higher shape anisotropy than the quasi spherical nickel aggregates.[21] Therefore, if one takes into account that the coercivity of a particular material is the result of the competition of the effect of the number of domains in the sample with the anisotropy of the sample, both depending on the size of the NPs, it becomes evident that the balance between both effects is maximized in the cubic morphology. [25,31-33]

As stated above the M_s value obtained for the four characterized Ni^0 nanoparticles are lower than the observed for bulk nickel (55 emu g^{-1}), but the lowest M_s value of 43 emu g^{-1} is presented by the flower-like particles of **Ni-4**. The decrease of the M_s value for the nickel nanoflowers has been explained by other authors taking into account the possibility that the increase in the surface area and the magnetic interaction between the petals in the nickel flowers may reduce the total magnetic moment at a given field, resulting in a lower M_s value. In addition, nickel nanoflowers with an average diameter of ~1.5 μm and thickness of 10 nm reported by Guan et al.[21] have a H_c of 170 Oe and remnant magnetization of 16.4 emu g^{-1}, while the reported by Kong et al.[26] with a diameter of 2-3 μm and thickness of 10-40 nm present a H_c = 323 Oe and M_r= 15.4 emu g^{-1}. These reported values are greater than the obtained for the as synthesized nickel flower-like aggregates (**Ni-4**), whose diameter is 2 μm and the thickness varies between 110-200 nm, giving values of H_c = 99 Oe and M_r =7 emu g^{-1}. This permits to infer that the thicknesses of the plates, which are forming the nanoflowers, seems to have an important role in the coercivity and remanent magnetization values.

Conclusions

In this paper we report a synthetic method which permits to obtain stable *fcc*-Ni^0 nanocrystals. The synthesized nickel nanocrystals present spherical, cubic and polyhedral aggregates; when the spherical NPs are subsequently heated under solvothermal conditions the modification of the morphology generates nickel flower-like 3D structures. The latter are generated without any change in the oxidation state of the metal.

Magnetic measurements of the synthesized nickel nanostructures show in all cases an enhanced ferromagnetic behaviour respect to the bulk nickel, obtaining values ranging from 73 till 200 Oe, which are greater than 0.7 Oe observed for bulk nickel. Although the coercivity is dependent of the size, surface area, magnetocrystalline and shape anisotropies, in the present study the different shapes of the nanoparticles, resulting in different anisotropies and dipolar interactions, seem to be the main factor influencing the coercivity values of these as-synthesized particles.

Acknowledgements

The authors acknowledge financial support from FONDECYT 1090477, 1110252, DI-104-12/R, Proyecto Basal CEDENNA, Financiamiento Basal FB0807 and grant ICM P10-061-F by FIC MINECOM. C.C. thanks CONICYT for the Doctoral fellowship 21110032.

Notes and references

[a] Universidad Andres Bello, Departamento de Ciencias Químicas, Santiago, Chile,
Fax: 56 2661 8269; Tel: 56 2770 3434; E-mail: vparedes@unab.cl.
[b] Centro para el Desarrollo de la Nanociencia y Nanotecnología, CEDENNA, Chile.
[c] Facultad de Ciencia, Universidad de Santiago de Chile,USACH, Chile.
[d] Facultad de Química y Biología, Universidad de Santiago de Chile, USACH, Chile.
[e] Facultad de Ciencias Químicas y Farmacéuticas, Universidad de Chile, Chile.
[f] Microscopy and Imaging Center and Materials Science and Engineering Program, Texas A&M University, College Station, TX 77843, USA.
[g] Department of Chemistry and Physics, Fayetteville State University, Fayetteville, NC 28301, USA

Electronic Supplementary Information (ESI) available: Fig. S1 EDX spectra of the synthesized Ni0 particles. (a) Ni-1; (b) Ni-2; (c) Ni-3; (d) Ni-5. Fig. S2: Figure S2. EDX spectra of the Ni-1. (a) sketch zone; (b) petals zone. Fig. S3: (a) FTIR spectrum of the synthesized Ni^0 particles. (b) DRIFT spectum of the synthesized Ni^0 particles. See DOI: 10.1039/b000000x/

References

1 Y. Shin, I.T. Bae, B.W. Arey and G.J. Exarhos, *Mater. Lett.*, 2007, 61, 3215.

2 (a) S.S. Abramchuk, D.A. Grishin, E.Y. Kramarenko, G.V. Stepanov and A.R. Khokhlov, *Polymer Science Series A*., 2006, 48, 138. (b) J. Schloesser, J. Roesler and D. Mukherji, *Int. J. Mat. Res*., 2011, 102, 532. (c) S. R. Bakshi, D. Lahiri and A. Agarwal, *Int. Mat. Rev.*, 2010, 55, 41. (d) M. Younas, M. Nadeen, M. Atif and R. Grossinger, *J. Appl. Phys.*, 2011, 109, 093704. (e) Y. Sengrong and C. Lloyds. *ACS Appl. Mat. Interf,*. 2010, 2, 616. (f) A.T. Raghavender and H.H. Nguyen, *J. Mag. Mag. Mat.* 2011, 323, 2145.

3 (a) Y.L. Hou and S. Gao, *J. Alloys Compd.*, 2004, 365, 112. (b) H. Zabel, *Superlattice. Micros.*, 2009, 46, 541. (c) S.A. Rawat, *J. Nanopart. Res*., 2011, 13, 5265. (d) Chen, K.T. Chan, J.J. Kan, C. Doran, O.Y. Lu, D.J. Smith, J. David and E.E. Fullerton, *Nano Lett.*, 2010, 10, 5070. (e) I. Betancourt and H.A. Davies, *Mater. Sci. Technol*., 2010, 6, 5. (f) Y. Hou, H. Kondoh, T. Ohta and S. Gao, Appl. Surf. Sci. 2005, 241, 218. (g) Y. Hou and Gao J. Mater. Chem. 2003, 13, 1510.

(a) M. Popovici, M. Gich and C. Savii, *Romanian Reports in Physics*, 2006, 58, 369. (b) A.C. Johnston-Peck, J.W. Wang, J.B. Tracy and B. Joseph, *ACS Nano*., 2009, 3, 1077. (c) H.Y. Wang, X.W. Chen, B.H. Zhou, W.H. Liao and G.H. Zhou, *Physica B-Condensed Matter.*, 2011, 406, 4407. (d) Y.T. Chen and J.W. Wu, *J. Alloys Compounds.*, 2011, 509, 9246. (e) A.C. Johnston-Peck, J.W. Wang and J.B. Tracy, *ACS Nano*., 2009, 3, 1077. (f) R. Wei, H. Yang, K. Du, W. Fu, Y. Tian, Q. Yu, S. Liu, M. Li and G. Zou, *Mat. Chem. Phys.*, 2008, 108, 188. (g) S. Ghosh, K. Das, K. Chakrabarti and S. K. De, *Cryst. Eng. Comm*, 2012, 14, 929.

5 (a) D.X. Tian and J.J. Zhao, *J. Comput. Theor. Nanosci.*, 2009, 6, 318. (b) N. Sounderya and Y. Zhang, *Recent Patents on Biomedical Engineering.*, 2008, 1, 34. (c) S. Laurent, D. Forge, M. Port, A. Roch, C. Robic, L. Vander Elst and R.N. Muller, *Chem. Rev.*, 2008, 108, 2064. (d) J. Gao, H. Gu and B. Xu, *Acc. Chem. Res*., 2009, 42, 1097. (e) B. Cedric, G. Thierry and A. Antigoni. *ACS Nano*., 2011, 5, 8488. (f) T.H. Tran and T.D. Nguyen, *Colloids Surf. B*., 2011, 88, 1. (g) T. Kitaoka, S. Yokota, M. Opietnik and T. Rosenau, *Mater. Sci. Eng. C*. 2011, 31, 1221.

6 (a) T. Neuberger, B. Schopf, H. Hofmann, M. Hofmann and B. von Rechenberg, *J. Magn. Magn. Mater.*, 2005, 293, 483. (b) A. Ito, M. Shinkai, H. Honda and T. Kobayashi, *J. Biosci. Bioeng.*, 2005, 100, 1. (c) J.H. Mi, S.T. Kim, J.S. Lee, K. Kim, J.H. Wu, J. Jeong, A.Y. Song, K.M. Lee and Y.K. Kim, *J. Appl. Phys.*, 2011, 109, 07B309. (d) N. Butoescu, C.A. Seemayer, M. Foti, O. Jordan and E. Doelker. *Biomaterials.*, 2009, 30, 1772. (e) C. Martinez-Boubeta, L. Balcells, R. Cristofol, C. Sanfeliu, E. Rodriguez, R. Weissleder, S. Lope-Piedrafita, K. Simeonidis, M. Angelakeris, F. Sandiumenge, A. Calleja, L. Casas, C. Monty and B. Martinez, *Nanomed. Nanotech. Biol. Med*., 2009, 6, 362. (f) V. Amendola, M. Meneghetti, G. Granozzi, S. Agnoli, S. Polizzi, P. Riello, A. Boscaini, C. Anselmi, G. Fracasso, M. Colombatti, C. Innocenti, D. Gatteschi and C. Sangregorio, *J. Mat. Chem.*, 2011, 21, 3803.

7 (a) W. Tang, W. Lu, X. Luo, B.S. Wang, X.B. Zhu, W.H. Song, Z.R. Yang and Y.P. Sun, *J. Magn. Magn. Mater*., 2010, 322, 2360. (b) R. Skomski, C. Binek, T. Mukherjee, S. Sahoo and D.J. Sellmyer, *J. Appl. Phys.* ,2008, 103, 07b329. (c) W. Tang, W.J. Lu, X. Luo, B.S. Wang, X.B. Zhu, W.H. Song, Z.R. Yang and Y.P. Sun, *Phys. B-Condens. Matter.*, 2010, 405, 2733. (d) X.C. Zhong, P.F. Tang, Z.W. Liu, D.C. Zeng, Z.G. Zheng, H.Y. Yu, W.Q. Qiu and Z.M. Zou, *J. Alloys Compd.*, 2011, 509, 6889. (e) Q. Luo and W.H. Wang. *J. Alloys Compd.*, 2010, 495, 209. (f) C. Krishnamoorthi, S.K. Barik and R. Mahendiran, *Solid. State. Commun*. 2011, 151, 107.

8 (a) S. Sun and C.B. Murray, *J. Appl. Phys*., 1999, 85, 4325. (b) C. Petit, A. Taleb and M. Pileni, *J. Phys. Chem*. B, 1999, 103, 1805. (c) M. Green and P. O'Brien, *Chem. Commun*., 2001, 1912. (d) X.G. Li, S. Takahashi, K. Watanabe, Y. Kikuchi and M. Koishi, *Nano Lett*., 2001, 1, 475. (e) N. Cordente, M. Respaud, F. Senocq, M.-J. Casanove, C. Amiens. B. Chaudret, *Nano Lett.*, 2001, 1, 565. (f) S.J. Park, S. Kim, S. Lee, Z.G. Khim, K. Char and T. Hyeon, *J. Am. Chem. Soc*., 2000, 122, 8581. (g) Y.P. Sun, H.W. Rollins and R. Guduru, *Chem. Mater*., 1999, 11, 7.

9 J.L. Morán-López, *Revista Mexicana de Física*, 2007, S53, 37.
10 Z. Y. Zhong, Z. T. Xiong, L. F. Sun, J. Z. Luo, P. Chen, X. Wu, J. Lin and K. L. Tan, *J. Phys. Chem. B*, 2002, 106, 9507.
11 G.H. Lee, S.H. Huh, J.W. Jeong and H.-C. Ri, *J. Magn. Magn. Mater*., 2002, 246, 404.
12 J.. Jung, K.-H. Choi, W.-S.Chae, Y.-R. Kim, J.-H. Jun, L. Malkinski, T. Kodenkandath, W. Zhou, J. B. Wiley and C.J. O'Connor, *J. Phys. Chem. Solids*., 2003, 64, 385.
13 D.J. Suh, T.-J. Park and J.-H. Kim, *J. Non-Cryst.Solids*., 1998, 225, 168.
14 S. Krompiec, J. Mrowiec-Białon, K. Skutil, A. Dukowicz, L. Pajak and A.B. Jarzebski, *J. Non-Cryst. Solids*., 2003, 315, 297.
15 S.-H. Lee, D.J. Suh, T.-J. Park and K.-L. Kim, *Catal. Commun.*, 2002, 3, 441.
16 (a) G. Ennas, A. Mei, A. Musinu, G. Piccaluga, G. Pinna and S. Solinas, *J. Non-Cryst. Solids*, 1998, 232–234, 587. (b) R. Luque, A.M. Balu, J.M. Campelo, C. Gonzalez-Arellano, M.J. Gracia, D. Luna, J.M. Marinas and A.A. Romero, *Mat. Chem. Phys.*, 2009, 117, 408.
17 (a) Y.D. Li, L.Q. Li, H.W. Liao and H.R. Wang, *J. Mater. Chem*., 1999, 9, 2675. (b) S. Gao, J. Zhang, Y.F. Zhu and C.M. Che, *New J. Chem*., 2000, 24, 739.
18 Z.P. Luo, *Acta Mater*., 2006, 54, 47.
19 (a) I.F. Trotter, H.W.Thompson and F. Works., *Biochem. J.*,1948, 42, 601. (b) S. Solliard, *Surf. Sci.*, 1981, 106, 58. L.S. Birks and H. Friedman, *J. Appl. Phys*., 1946, 17, 687.
20 H. Li, J. Liao, X. Zhang, X. Lu, J. Liang, Y. Feng and S. Yu, *Aust. J. Chem*., 2011, 64, 1494.
21 (a) J. Guan, L. Liu, L. Xu, Z. Sun and Y. Zhang, *Crys. Eng. Comm*., 2011, 13, 2636. (b) F. Jia, L. Zhang, X. Shang, Y. Yang. *Adv. Mater*. 2008, 20, 1050.
22 W. Xu, K.Y. Liew, H. Liu, T. Huang, Ch. Sun and Y. Zhao, *Mater. Lett.*, 2008, 62, 2571.
23 Z. An, S. Pan and J. Zhang, *J. Phys. Chem. C*., 2009, 113, 2715.
24 S. Senapati, S.K. Srivastava, S.B. Singh and K. Biswas, *Cryst. Growth. Des*., 2010, 10, 4068.
25 D.E. Zhang, E. Yang, M.Y. Wang, X.B. Zhang, S.Z. Li, G.Q. Han, A.L. Ying and Z.W. Tong, *J. Phys. Chem. Solids*., 2011, 72, 1397.
26 J. Kong, W. Lu, F. Wang, X. Wang, L. Luan, J. liu, Y. Wang, Z. Zhang, M. Itoh and K.I. Machida, *J. Solid. State Chem*., 2011, 184, 2994.
27 J. Ye, Q.W. Chen, H.P. Qi and N. Tao, *Cryst. Growth. Des*., 2008, 8, 2464.
28 X.M. Ni, Q.B. Zhao, D.E. Zhang, X.J. Zhang and H.C. Zheng, *J. Phys. Chem C*, 2007, 111, 601.
29 A. Mathews, N. Munichandraiah and G.M. Rao, *Mater. Sci. Eng. B*, 2009, 158, 7.
30 J.H. Hwang, V.P. Dravid, M.H. Teng, J.J. Host, B.R. Elliot, D.L. Johnson and T.O. Mason, *J. Mater. Res*., 1997, 12, 1076. (b) S. Zhang, X, Chen, X. Zhang and Ch. Shi, *Solid State. Commun*., 2006, 139, 403.
31 D.L. Leslie-Pelecky and R.D. Riecky. *Chem. Mater*., 1996, 8, 1770.
32 H.O. Cao, Z. Xu, H. Sang, D. Sheng and C.Y. Tie, *Adv. Mater*., 2001 13, 121.
33 T.M. Whitney, J.S. Jiang, P.C. Searson and C.L. Chien, *Science*, 1993, 261, 1316.

Graphical Abstract

Effect of the Different Synthetic Parameters on the Morphology and Magnetic Properties of Nickel Nanoparticles

Veróonica Paredes-García, Carlos Cruz, Néstor Toledo, Juliano Denardin, Diego Venegas-Yazigi, Carolina Castillo, Evgenia Spodine and Zhiping Luo

Stable spherical Ni(0) nanoparticles can be reheating modifying the morphology of these for obtain flower-like Ni(0) arrangements, retaining the highly crystallinity and without the oxidation of the nanoparticles.